Equation Chapter 1 Section 1

Power adjustment and measurement with square-wave phase grating controlled by LCSLM

Jian Zhang[1], Xiang Liu[1], Liying Wu[1,#], Yu Gan[1], Dong Wang[1], and Jiajia Ge[2]

1 Institute of Ultra-Precision Optoelectronic Instrument Engineering, Harbin Institute of Technology, #2 Yikuang Street, Harbin, 150080, China
2 Patent Examination Cooperation Center of SIPO, Box 43 in Building 4th, #18 Zhongguancun Nansi Street, Beijing, 100190, China
Corresponding Author / E-mail: wly1024@126.com ; Wly1024@hit.edu.cn, TEL: +86-451-8640-2208 ext. 809, FAX: +86-451-8640-2258

KEYWORDS : phase grating, liquid crystal spatial light modulator, optical tweezers, power control

Holographic optical tweezers controlled by a liquid crystal spatial light modulator (LCSLM) is not only a noncontact tool to dynamically manipulate cells and biomolecules in real time, but also a tool for bio-measurement with high performance. The performance can be related to the power-adjustment accuracy of the optical tweezers, which originally is a laser spot focused in three dimensions. Multiple 3D laser spots generate multiple optical tweezers. In order to be able to control the power of these optical tweezers with high accuracy and to make it suitable for real-time LCSLM-controlled bio-measurement, a square-wave phase grating is proposed to adjust the power of these laser spots generated by a LCSLM. After being normalized in the range of 0-1, the power can be controlled by changing the phase depth of the proposed grating. As there is only one variable in the grating, the phase depth can be calculated in about 3 microseconds by Matlab software directly. By optimization of phase depth, the influence from the phase encoding error of LCSLM has been suppressed, the accuracy is improved, and a simulated resolution of normalized power 0.002 has been proved through experiments.

Manuscript received: January XX, 2011 / Accepted: January XX, 2011

NOMENCLATURE

φ = phase depth of the square-wave phase grating
M = the number of linear phase levels between 0 and 2π achieved by the LCSLM
P_{norm} = normalized power of laser spot(s)
ΔP_{max} = maximal power-normalized step
N = the number of linear normalized power
ε = error of the normalized power
δ = resolving error of the normalized power
ξ, η = spatial-frequency coordinates of the system
z = axial coordinate of the system

1. Introduction

Micron-sized particles can be manipulated by the force of radiation pressure from laser spots[1]. In 1998, Hayasaki and co-authors[2], introduced a liquid crystal spatial light modulator (LCSLM) into an optical system for noncontact manipulation. With controllable feature, the LCSLM can be used to dynamically generate multiple laser spots[3] in three dimensions in order to manipulate cells and biomolecules in real time.

As a noncontact tool of optical manipulation, optical tweezers also can be a powerful transducer used for bio-measurement at the same time, such as high-sensitivity measurement of free-protein concentration [4], sub-pico-newton force measurement[6, 7], in-vitro Raman-spectroscopy measurement of living cells[5] and so on. In these measurements, the adjustable laser power of optical tweezers can play an important role to improve the measurement performances, method, accuracy and so on. For example, in Ref. [4] a power-linearly-ramped laser is used to improve the sensitivity of measuring free-protein concentration.

For a LCSLM-based optical tweezers system, the method of adjusting the intensity incident on the LCSLM has been used in many applications to gain adjustable input power. With this method, one option is to tune the driver of a laser source[6], while the problem is that the stability of laser intensity usually is poor, typically 2-5%, sometimes the intensity profile is even changed during the adjusting[7]. To solve the problem, a tunable optical

component, such as adjustable attenuator or acousto-optical modulator, can be put in front of the laser source[4, 8]. However, the additional optical component incorporated into the LCSLM-based system does not only inevitably cause an insertion loss, but also makes the system more complex and expensive. The better method is to use LCSLM self, which can be achieved by computer generated hologram (CGH) algorithms[9]. After being compared with many CGH algorithms, Weighted Gerchberg-Saxton (GSW) has the most advantages to adjust the intensity of any one spot with high accuracy in real time by tuning the relative intensities of spots, because the GSW can obtain low relative-intensity error and high diffraction efficiency in only 10 iterations. However, the phase encoding error of a LCSLM degrades the accuracy of intensities to 4% from the simulation result 1%. In theory, axial-displacement method[10] can easily and perfectly suppress the inaccuracy of the relative intensities, except for the inaccuracy of the diffraction efficiency. The power of 3D laser spots is thus still hard to be controlled by a LCSLM with high-accuracy in real time. A tunable square-wave phase grating is proposed to adjust the total power of these spots.

2. Power adjustment

2.1 Square-wave phase grating

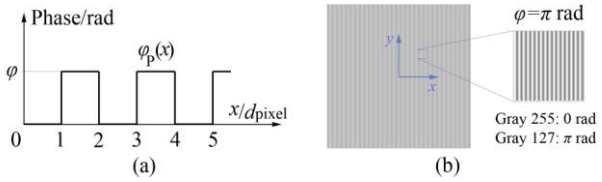

Fig. 1. Square-wave phase grating. (a) Phase profile. (b) 2D gray image controlled by a LCSLM.

The total-power adjustment of 3D laser spots is accomplished via the square-wave phase grating $\exp[i\varphi_P(x)]$ shown in Fig. 1 above. In order to yield a maximal angle of view, the period of the grating is made to be two pixel widths $2d_{pixel}$, during which one pixel is modulated to phase zero and the other to phase φ.

Supposing that a plane wave with wavelength λ is normally incident on grating $\exp[i\varphi_P(x)]$, according to Fraunhofer diffraction integral in spite of constant coefficient[11], the diffraction complex amplitude of the grating can be written as

$$U(\xi)=\mathcal{F}\left[e^{i\varphi_P(x)}\right] =\frac{1}{2}\sum_{n=-\infty}^{\infty}\delta\left(\xi-\frac{n}{2d_{pixel}}\right)\mathrm{sinc}\left(\frac{n}{2}\right)\left(1+e^{i\varphi}e^{in\pi}\right)e^{\frac{in\pi}{2}} \quad (1)$$

where $\mathcal{F}[\bullet]$ represents Fourier Transform, ξ the spatial frequency, n the number of diffraction order and $\mathrm{sinc}(x)=\sin(\pi x)/(\pi x)$.

The efficiency η^n of diffractive n-th order is given by the squared modulus of the n-th-order coefficient in Eq.(1), thus, the diffraction efficiency of 0-th order is

$$\eta^0(\varphi)=(1+\cos\varphi)/2 \quad (2)$$

The diffraction efficiency is commonly defined as

$$\eta^0(\varphi)=P_0/P_{inc} \quad (3)$$

where P_0 is diffractive 0-th-order power of the square-wave grating, and P_{inc} the laser power incident on the grating, i.e., the LCSLM in this paper.

The power of diffractive 0-th order P_0 is thus described by

$$P_0=P_{inc}(1+\cos\varphi)/2 \quad (4)$$

Since P_{inc} is a constant power, the power P_0 can be continuously adjusted in range from 0 to the maximal power P_{inc} just by modulating its phase depth φ.

2.2 Power of a single 3D laser spot

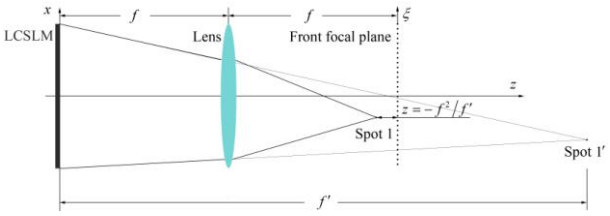

Fig. 2. Schematic diagram of Fourier optics propagation from the LCSLM plane (back focal plane) to imaging plane.

In a holographic-optical-tweezers system [3, 10], where a LCSLM is commonly placed in a plane conjugate to the input pupil of a lens such as a microscope, a phase hologram $\exp[i\varphi(x, y)]$ displayed on the LCSLM can be used to transform an incident laser beam into a single 3D laser spot. This spot can be generated by a beam with a quadratic phase factor, i.e. it acts as the point source of a converging spherical wave. For example, just away from the LCSLM with a quadratic phase factor $\exp\left[-i\pi\left(x^2+y^2\right)/(\lambda f')\right]$, a beam would focus at spot $1'$ at distance f' from the LCSLM plane, as shown in Fig. 2 above. The complex amplitude of spot $1'$ can be expressed as[12]

$$U_{1'}(\xi',\eta')=\mathcal{F}\left[e^{i\varphi(x,y)}e^{\frac{i\pi}{\lambda f'}(x^2+y^2)}\right] \quad (5)$$

where (ξ',η') is the spatial-frequency coordinates of spot $1'$.

Then a lens with focal length f images spot $1'$ to spot 1 at position $z=-f^2/f'$ from the front focal plane of the lens, as reported in [10], the complex amplitude of spot 1 can be expressed by

$$U_1(\xi,\eta,z)=\mathcal{F}\left[e^{i\varphi(x,y)}e^{\frac{-i\pi z}{\lambda f^2}(x^2+y^2)}\right] \quad (6)$$

where (ξ, η) is the spatial-frequency coordinates with unit $\lambda f/D$, D is the aperture of the LCSLM and z the axial coordinate from the front focal plane.

In order to adjust the power of the 3D laser spot generated by phase hologram $\exp[i\varphi_H(x, y)]$, a composite phase profile displayed on a LCSLM is gained directly by adding the phase profile of square-wave phase grating $\exp[i\varphi_P(x)]$ to original phase hologram $\exp[i\varphi_H(x, y)]$ as,

$$\varphi(x,y)=\varphi_H(x,y)+\varphi_P(x) \quad (7)$$

After Fourier transform in the form of Eq.(6), the complex amplitude of spot 1 can be changed to

$$U_1(\xi,\eta,z)=\mathscr{F}\left[e^{i\varphi_H(x,y)}e^{\frac{-i\pi z}{\lambda f^2}(x^2+y^2)}\right] *\frac{1}{2}\sum_{n=-\infty}^{\infty}\delta\left(\xi-\frac{n}{2d_{\text{pixel}}}\right)\text{sinc}\left(\frac{n}{2}\right)\left(1+e^{i\varphi}e^{in\pi}\right)e^{\frac{in\pi}{2}} \quad (8)$$

where (ξ_1, η_1) is the spatial-frequency coordinates of spot $1'$, and $*$ presents convolution operation.

And the diffraction efficiency of the original spot 1 governed by diffractive 0-th order of the grating becomes

$$\eta^1=\eta_H^1(1+\cos\varphi)/2 \quad (9)$$

where η_H^1 is the diffraction efficiency of the laser spot 1 governed by the original phase hologram $\exp[i\varphi_H(x, y)]$.

The power of spot 1 can be described by

$$P(\varphi,\xi_1,\eta_1,z_1)=P_{\text{inc}}\eta_H^1(1+\cos\varphi)/2 \quad (10)$$

Its normalized power governed by the square-wave phase grating can thus be depicted as

$$P_{\text{norm}}(\varphi,\xi_1,\eta_1,z_1)=(1+\cos\varphi)/2 \quad (11)$$

2.2 Power of multiple 3D laser spots

The phase hologram $\exp[i\varphi_H(x, y)]$ displayed on the LCSLM can also be used to generate multiple laser spots with individual quadratic phase factors. As described by Ref. [12], the complex amplitude of the m-th spot $U_m(\xi, \eta, z)$ can be individually calculated by Eq.(6). After the phase profile of a square-wave phase grating $\varphi_P(x)$ is added into the original phase profile $\varphi_H(x, y)$ by Eq.(7), the composite phase profile $\varphi(x, y)$ can also be gained. Same with Eq.(10), the power of m-th laser spot (ξ_m,η_m,z_m) can be expressed as

$$P(\varphi,\xi_m,\eta_m,z_m)=P_{\text{inc}}\eta_H^m(1+\cos\varphi)/2 \quad (12)$$

where η_H^m is the diffraction efficiency of m-th spot governed by the original phase hologram $\exp[i\varphi_H(x, y)]$.

The total power of all concerned spots can be thus described as

$$\sum_{m=1}^{Num}P(\varphi,\xi_m,\eta_m,z_m)=\sum_{m=1}^{Num}\eta_H^m P_{\text{inc}}(1+\cos\varphi)/2 = P_{Num}(1+\cos\varphi)/2 \quad (13)$$

where Num is the number of all concerned spots, P_{Num} is the original total power of all concerned spots governed by phase hologram $\exp[i\varphi_H(x, y)]$.

We just concentrate in this paper on the adjustment ability using a square-wave phase grating; the total power of all concerned spots is thus normalized to

$$P_{\text{norm}}(\varphi)=(1+\cos\varphi)/2 \quad (14)$$

When the number of spots Num is equal to 1, the normalized power (14) is equivalent to Eq.(11). It can be seen through analyses in section 2.1 that a square-wave phase grating generates a power-controllable diffractive zero order, which can be used to adjust the power of 3D spots generated by original phase hologram $\exp[i\varphi_H(x, y)]$. However, in order to avoid the overlap of the concerned spots controlled by the other diffractive orders of the grating ($n\neq0$) in Eq.(8), the two-pixel period structure of the square-wave phase grating makes the maximal angle of view to be reduced by 1/2 to $(-D/(4d_{\text{pixel}}), D/(4d_{\text{pixel}}))$ in the direction ξ.

2.3 Power adjustment

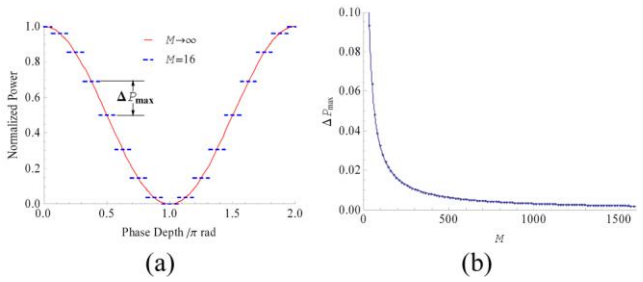

Fig. 3. Normalized power adjusted by a square-wave phase grating

The adjustment using Eq.(14) is symmetrical to π radian in [0, 2π] and changed monotonically from 1 to 0 in [0, π], as shown by the solid line in Fig. 3 (a). However, a LCSLM only allows M linear phase levels between 0 and 2π, and it makes the square-wave phase grating to adjust the power with steps in reality, as shown by the dashed line in Fig. 3 (a). Meanwhile, the maximal power step $\Delta P_{\max}$, decreasing with number M described in Fig. 3 (b), is inverse proportion to a power-adjustment resolution. And in the constraint of the absolute value of power error ε smaller than $\Delta P_{\max}/2$, the normalized power resolution of 0.002 is expected with a LCSLM of M=1600, as shown in Table. 1. Furthermore, a desired phase depth φ of the grating can be accurately calculated by equation (14) in on the average of 3 μs via Matlab software in PC with 2.8GHz Intel Pentium D 820 CPU and 512MB Memory.

Table. 1. Simulation results of adjusting the normalized power

M	16	256	314	1024	1600
$\Delta P_{\max}$	0.1913	0.0123	0.0100	0.0031	0.0020
N	5	81	100	332	500
ε	0.0913	0.0061	0.0050	0.0015	0.0010

3. Experiments

3.1 Setup and principle of measurement

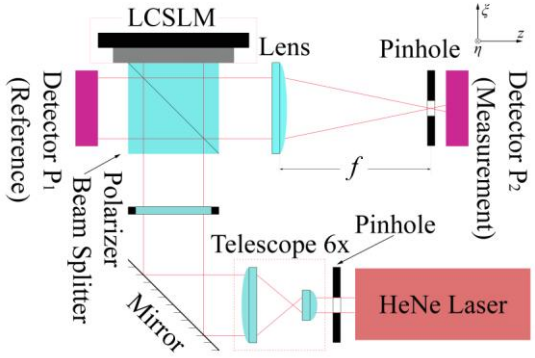

Fig. 4. Measurement setup, LCSLM is placed in the back focal plane of the lens.

A LCSLM (BNS, P512-0635-DVI, M=1600, d_{pixel}=15 μm and D =7.68 mm) is used to generate the composite phase profile (7) moduled by 2π due to the limited phase modulation depth of a typical LCSLM. As shown in Fig. 4, the polarization direction of the polarizer must be parallel to the liquid crystal director of the LCSLM in order to achieve a phase-only modulation. A 5mm-

diameter expanded beam originating from a frequency-stabilized laser (λ=632.8 nm, 2 mW) is incident on the LCSLM, subsequently away from the LCSLM, and focused into laser spots by a lens with f=150 mm. One of these spots is sampled by a pinhole of 0.6 mm in diameter and measured by a dual-channel power meter (Newport 2832-C), where one channel measures the power of the sampled spot P_2 and the other measures a branch power of the laser source P_1 as a reference to eliminate the power-instability effect from the laser source. Only one individual laser spot can be measured each time, multiple spots can thus be measured one-by-one.

The measured power P_1 can be described by the power of laser source P_{laser} as

$$P_1 = a_1 P_{\text{laser}} \tag{15}$$

where a_1 is the power-transferred coefficient for the reference branch, which is governed both by the reflectance of the beamsplitter and by the transmittance of the telescope and the polarizer.

The measured power P_2 can be described as

$$P_2 = a_2 P_{\text{norm}}(\varphi) \sum_{m=1}^{Num} \eta_{\text{H}}^m P_{\text{laser}} \tag{16}$$

where a_2 is the power-transferred coefficient for the measurement branch, which is governed both by the reflectance of the beamsplitter and by the transmittance of the telescope, the polarizer, the beamsplitter and lens.

The normalized power $P_{\text{norm}}(\varphi)$ we concerned can be thus expressed as

$$P_{\text{norm}}(\varphi) = \frac{a_1}{a_2 \sum_{m=1}^{Num} \eta_{\text{H}}^m} \times \frac{P_2}{P_1} \tag{17}$$

For fixed spots, the coefficient in front of P_2/P_1 is a constant; the normalized efficiency can thus be calculated by the normalized value of P_2/P_1, which can not be affected by the laser power P_{laser}.

3.2 Measurement results of a single laser spot

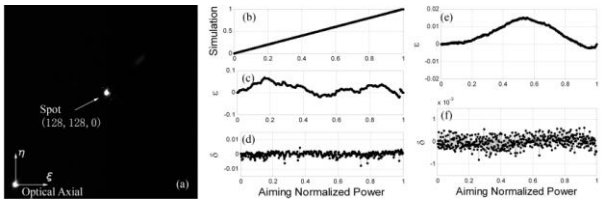

Fig. 5 Linearly adjusting the power of a single spot at (128, 128, 0 mm) via the composite phase (7) with φ in 0-π. (a) Diffraction image captured by a CCD (PointGrey GRAS-20S4M-C) placed in the front focal plane of lens in Fig. 4. (b) 500 linear resolved powers simulated are normalized by its maximal power. (c) Achieved by the LCSLM in Fig. 4, the errors of normalized powers are in ±0.0673, and (d) the resolving errors of normalized powers are in ±0.0080. After shifting the spot along the optical axial to z_1=-20 mm, (e) the errors of measured normalized powers are in ±0.0151, and (f) their resolving errors are in ±0.0008.

As shown in section 1, due to the phase encoding errors of the LCSLM, the adjustment of normalized power of the laser spot in the front focal plane of lens presents an intolerable error ε and resolving error δ about one order of the desired accuracy, as shown in Fig. 5 (c) and (d). Both of the errors can be suppressed by the axial-displacement method[10]. Especially, the resolving errors δ can be suppressed enough for the desired resolution, such as δ in ±0.0008 for a resolution of 0.002 described in detail in Fig. 5 (f), however, the error ε is still over one order of the error constraint ±0.001. In theory, there are still 1100 phase levels unused as a higher-resolution optimization domain for M=1600 & N=500 with the phase depth φ in the range from 0 to 2π. For the laser spot having resolving error δ in ±0.001, 500 equidistant normalized powers could be achieved by compensating the error with the optimized phase levels, as shown in Fig. 6. And similar results can be also achieved at other spot out of the front focal plane of the lens (z≠0), described in detail in Table. 2.

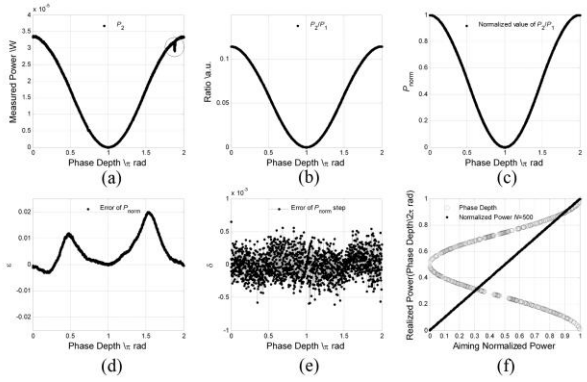

Fig. 6 Power resolution of a spot at (128, 128, -20 mm) improved by 1600 linear phase levels in the range of 0-2π. (a) Measured power P_2. (b) Ratio of the measured power P_2 and P_1 can eliminate the power-instability effect marked by a circle in (a). (c) The ratio of P_2/P_1 is normalized in the range of 0-1. (d) The absolute value of errors of the normalized power $|\delta|$ are in ±0.02, and (e) the absolute value of resolving errors $|\varepsilon|$ are in ±0.0007. (f) 500 linear resolved normalized powers can be achieved by optimizing the phase depth of the grating.

Table. 2 Measurement results of single laser spot out of the front focal plane of the lens

z_1 /mm	Position (ξ_1,η_1)	$\lvert\varepsilon\rvert^*$ /10^{-3}	$\lvert\delta\rvert$ /10^{-4}	N	Position (ξ_1,η_1)	$\lvert\varepsilon\rvert^*$ /10^{-3}	$\lvert\delta\rvert$ /10^{-4}	N
	(0,0)	74.6	10	500	(128,128)	11.7	7	500
-10	(64,128)	22.6	7	500	(192,128)	20.1	8	500
	(128,64)	12.8	6	500	(128,192)	15.1	8	500
	(0,0)	66.2	11	500	(128,128)	19.9	7	500
-20	(64,128)	31.8	7	500	(192,128)	39.1	9	500
	(128,64)	21.3	7	500	(128,192)	20.7	11	500

* Errors in phase depth [0,2π] before optimization.

3.2 Measurement results of 2x2 3D laser spots

As shown in Fig. 7 (a) and (b), a phase hologram calculated by the GSW[13] generates four equal-bright 3D spots, and their projections forms a 2x2 3D array and centered at the optical axial in the front focal plane. After a square-wave phase grating was added to the original hologram in the form of Eq. (7), the power of each spot was adjusted nearly synchronously, as shown in Fig. 7 (c). After being normalized in the range of 0-1, the total power is in good agreement with the simulation, as shown in Fig. 7 (d). Furthermore, as shown in Fig. 7 (e), most of the absolute value of

resolving error $|\delta|$ is less than 0.001, a normalized total power resolution of 0.002 can be obtained in the range of phase depth φ from 0 to π, as shown in Fig. 7 (f). And the similar results can also be achieved at other 2x2 spots with different three-dimension configures, described in detail in Table. 3.

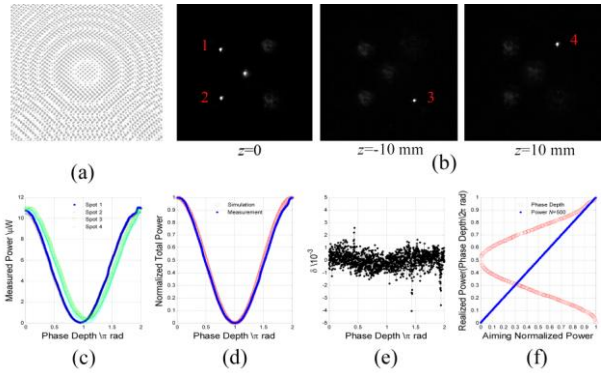

Fig. 7. 2x2 3D laser spots with projection spacing 64. Calculated by a 100-iteration GSW, the phase hologram (a) displayed by a gray image generates (b) laser spots captured by a CCD nearby the front focal plane of the lens in Fig. 4, and marked in turn by 1, 2, 3 and 4. (c) The powers of these 4 spots were adjusted synchronously, and (d) their total power, normalized in the range of 0-1, has (e) resolving errors in ±0.0041. (f) 500 linear normalized total powers can be achieved by optimizing the phase depth of the square-wave phase grating in the range of phase depth [0, 2π] in order to suppress the error of normalized power.

Table. 3. Measurement results of 2x2 laser spots

	Positions (ξ_m, η_m, z_m) of 4 spots marked in turn by m =				$\lvert\delta\rvert$ 10^{-3}	N
	1	2	3	4		
1	(64,64,0)	(64,-64,0)	(-64,-64,-1)	(-64,64,1)	11.2	498
2	(64,64,0)	(64,-64,0)	(-64,-64,-10)	(-64,64,10)	11.2	499
3	(64,64,0)	(64,-64,0)	(-64,-64,-20)	(-64,64,20)	7.3	499
4	(32,32,0)	(32,-32,0)	(-32,-32,-1)	(-32,32,1)	6.2	500
5*	(32,32,0)	(32,-32,0)	(-32,-32,-10)	(-32,32,10)	4.1	500
6	(32,32,0)	(32,-32,0)	(-32,-32,-20)	(-32,32,20)	7.5	500
7	(96,96,0)	(96,-96,0)	(-96,-96,-1)	(-96,96,1)	13.7	497
8	(96,96,0)	(96,-96,0)	(-96,-96,-10)	(-96,96,10)	3.6	499
9	(96,96,0)	(96,-96,0)	(-96,-96,-20)	(-96,96,20)	3.4	491

* Described in detail in Fig. 7.

4. Conclusions

A 50%-fill-factor square-wave phase grating is a viable choice for a LCSLM-based system to adjust the power of laser spots, which obeys a simple cosine function of the phase depth of the grating. And a desired phase depth can be obtained in 3 μs. Furthermore, experiments have demonstrated that the resolving error of normalized power is so less that a simulated resolution can be achieved by optimizing the phase depth of the grating. It would have potential applications in bio-measurement field to improve the measurement performance of a LCSLM-based system.

ACKNOWLEDGEMENT

This work is funded by National Natural Science Foundation of China under grant 60878048, and China Postdoctoral Science Foundation under grant 20080440898.

REFERENCES

1. Liesener J., Reicherter M., Haist T. and Tiziani H. J., "Multi-Functional Optical Tweezers Using Computer-Generated Holograms," Opt. Commun., Vol. 185, No. 1-3, pp. 77-82, 2000.
2. Hayasaki Y., Itoh M., Yatagai T. and Nishida N., "Nonmechanical Optical Manipulation of Microparticle Using Spatial Light Modulator," Opt. Rev., Vol. 6, No. 1, pp. 24-27, 1999.
3. Curtis J. E., Koss B. A. and Grier D. G., "Dynamic Holographic Optical Tweezers," Opt. Commun., Vol. 207, No. 1-6, pp. 169-175, 2002.
4. Akcakir O., Knutson C. R., Duke C., Tanner E., Mueth D. M., Plewa J. S. and Bradley K. F., "High-Sensitivity Measurement of Free-Protein Concentration Using Optical Tweezers," Proc. SPIE, Vol. 6863, pp. 686305, 2008.
5. Xie C. G., Goodman C., Dinno M. A. and Li Y. Q., "Real-Time Raman Spectroscopy of Optically Trapped Living Cells and Organelles," Opt. Express, Vol. 12, No. 25, pp. 6208-6214, 2004.
6. Pine J. and Chow G., "Moving Live Dissociated Neurons with an Optical Tweezer," IEEE T. Bio-med Eng., Vol. 56, No. 4, pp. 1184-1188, 2009.
7. Kennedy C. J., "Model for Variation of Laser Power with M^2," Appl. Optics, Vol. 41, No. 21, pp. 4341-4346, 2002.
8. Funk M., Parkin S. J., Stilgoe A. B., Nieminen T. A., Heckenberg N. R. and Rubinsztein-Dunlop H., "Constant Power Optical Tweezers with Controllable Torque," Opt. Lett., Vol. 34, No. 2, pp. 139-141, 2009.
9. Persson M., Engström D., Frank A., Backsten J., Bengtsson J. and Goksör M., "Minimizing Intensity Fluctuations in Dynamic Holographic Optical Tweezers by Restricted Phase Change," Opt. Express, Vol. 18, No. 11, pp. 11250-11263, 2010.
10. Lee S. H. and Grier D. G., "Robustness of Holographic Optical Traps against Phase Scaling Errors," Opt. Express, Vol. 13, No. 19, pp. 7458-7465, 2005.
11. Goodman J. W., "Introduction to Fourier Optics," McGraw-Hill, pp. 73-75, 1996.
12. Škereň M., Richter I. and Fiala P., "Design and Optimization Considerations of Multi-Focus Phase-Only Diffractive Elements," Proc. SPIE, Vol. 5182, pp. 233-242, 2003.
13. Engström D., Frank A., Backsten J., Goksör M. and Bengtsson J., "Grid-Free 3D Multiple Spot Generation with an Efficient Single-Plane FFT-Based Algorithm," Opt. Express, Vol. 17, No. 12, pp. 9989-10000, 2009.